

## NEUTRONIZATION DURING TYPE IA SUPERNOVA SIMMERING

ANTHONY L. PIRO<sup>1</sup> AND LARS BILDSTEN

Kavli Institute for Theoretical Physics, Kohn Hall, University of California, Santa Barbara, CA 93106;  
 piro@kitp.ucsb.edu, bildsten@kitp.ucsb.edu

*Accepted for publication in The Astrophysical Journal*

### ABSTRACT

Prior to the incineration of a white dwarf (WD) that makes a Type Ia supernova (SN Ia), the star “simmers” for  $\sim 1000$  years in a convecting, carbon burning region. We have found that weak interactions during this time increase the neutron excess by an amount that depends on the total quantity of carbon burned prior to the explosion. This contribution is in addition to the metallicity ( $Z$ ) dependent neutronization through the  $^{22}\text{Ne}$  abundance (as studied by Timmes, Brown, & Truran). The main consequence is that we expect a “floor” to the level of neutronization that dominates over the metallicity contribution when  $Z/Z_{\odot} \lesssim 2/3$ , and it can be important for even larger metallicities if substantial energy is lost to neutrinos via the convective Urca process. This would mask any correlations between SN Ia properties and galactic environments at low metallicities. In addition, we show that recent observations of the dependences of SNe Ia on galactic environments make it clear that metallicity alone cannot provide for the full observed diversity of events.

*Subject headings:* nuclear reactions, nucleosynthesis, abundances — supernovae: general — white dwarfs

### 1. INTRODUCTION

The use of Type Ia supernovae (SNe Ia) as cosmological distance indicators has intensified the need to understand white dwarf (WD) explosions. Of particular importance is the origin of the Phillips relation (Phillips et al. 1999), an essential luminosity calibrator. Recent models demonstrate that it can be explained by large variations in the abundance of stable iron group elements (Woosley et al. 2007) with the dominant cause for diversity likely residing in the explosion mechanism (Mazzali et al. 2007).

One additional variable is the metallicity of the WD core, which yields excess neutrons relative to protons due to the isotope  $^{22}\text{Ne}$ . This is usually expressed as

$$Y_e = \sum_i \frac{Z_i}{A_i} X_i, \quad (1)$$

where  $A_i$  and  $Z_i$  are the nucleon number and charge of species  $i$  with mass fraction  $X_i$ . The neutronization is critical for setting the production of the neutron-rich isotopes (Thielemann et al. 1986). If no weak interactions occur during the explosion, the mass fraction of  $^{56}\text{Ni}$  produced is simply  $X(^{56}\text{Ni}) = 58Y_e - 28$ , assuming  $^{56}\text{Ni}$  and  $^{58}\text{Ni}$  are the only burning products (Timmes et al. 2003). The neutronization also affects the explosive burning, including the laminar flame speed (Chamulak et al. 2007a). However, the metallicity range of progenitors is not large enough to account for the full SNe Ia diversity (see §4), making it critical to explore all factors that determine  $Y_e$ .

A potential neutronization site is the convective carbon burning core that is active for  $\sim 1000$  years prior to the explosion. The hydrostatic evolution associated with this simmering phase terminates when the core temperature is sufficiently high that burning is dynamical (Nomoto et al. 1984; Woosley & Weaver 1986; Woosley et al. 2004; Wunsch & Woosley 2004; Kuhlen et al. 2006), and a

flame commences (Timmes & Woosley 1992). We show here that protons from the  $^{12}\text{C}(^{12}\text{C}, p)^{23}\text{Na}$  reaction during simmering capture on  $^{12}\text{C}$ , and that subsequent electron captures on  $^{13}\text{N}$  and  $^{23}\text{Na}$  decrease  $Y_e$ . This process continues until either the explosion occurs or sufficient heavy elements have been synthesized that they capture the protons instead.

In §2, we present simmering WD core models and summarize the reaction chains that alter  $Y_e$ . We find that one proton is converted to a neutron for each six  $^{12}\text{C}$  nuclei consumed for burning at  $\rho < 1.7 \times 10^9 \text{ g cm}^{-3}$ . At densities above this, an additional conversion occurs from an electron capture on  $^{23}\text{Na}$ . Hence, the  $Y_e$  in the core depends on the amount of carbon burned during simmering and the density at which it occurs, which we quantify in §3. We find that neutronization during simmering dominates for metallicities  $Z/Z_{\odot} \lesssim 2/3$ . We conclude in §4 by discussing the observations and noting where future work is needed.

### 2. NEUTRON PRODUCTION DURING SIMMERING

Thermally unstable burning begins when the energy generation rate from carbon fusion,  $\epsilon$ , exceeds neutrino cooling (Nomoto et al. 1984). The thin solid lines in Figure 1 show the range of ignition curves for  $X(^{12}\text{C}) = X(^{16}\text{O})$  (Yakovlev et al. 2006) with the middle line the nominal current best. The carbon fuses via  $^{12}\text{C}(^{12}\text{C}, p)^{23}\text{Na}$  and  $^{12}\text{C}(^{12}\text{C}, \alpha)^{20}\text{Ne}$  with branching ratios of 0.44 and 0.56, respectively. At “early” times the liberated protons capture onto  $^{12}\text{C}$ , while at “late” times enough heavy elements ( $^{23}\text{Na}$  or  $^{23}\text{Ne}$ ) have been produced that they capture the protons instead.

We treat the evolution during the simmering phase as a series of hydrostatic models consisting of an adiabatic convective core and an isothermal surface at  $10^8 \text{ K}$ . As long as the convection zone is well described as an adiabat this is sufficient for resolving the thermal structure without the need to explicitly solve the energy transfer equation. These assumptions become weaker once the central temperature is  $T_c \gtrsim 7 \times 10^8 \text{ K}$ , so that burning occurs sufficiently quickly that there is considerable energy generation within a convective

<sup>1</sup> Current address: Astronomy Department and Theoretical Astrophysics Center, University of California, Berkeley, CA 94720; tpiro@astro.berkeley.edu

tive eddy overturn timescale (Garcia-Senz & Woosley 1995). The energy generation does come into play because it sets the heating timescale,  $t_h \equiv c_p T_c / \epsilon$ , where  $c_p$  is the specific heat of the liquid ions (we use linear mixing and the Coulomb energy from Chabrier & Potekhin 1998), nearly given by the classical Dulong-Petit law  $c_p \approx 3k_B / \mu_i m_p$ , where  $\mu_i$  is the ion mean molecular weight. Since we evaluate  $t_h$  using the central conditions it is a lower limit since it should include the entire heat capacity of the convective region (Piro & Chang 2007; see related discussion for neutron stars in Weinberg et al. 2006). In this way, for a given thermal profile there is a well-defined heating timescale, which connects our stationary models to the true time evolution. The thick dashed lines in Figure 1 trace out the trajectory of the central temperature,  $T_c$ , and density,  $\rho_c$ , for  $M = 1.35M_\odot$  and  $M = 1.37M_\odot$  (left and right, respectively), both using compositions of  $X(^{12}\text{C}) = 0.5$ ,  $X(^{16}\text{O}) = 0.48$ , and  $X(^{22}\text{Ne}) = 0.02$ . These indicate that  $\rho_c$  decreases with increasing  $T_c$  (Lesaffre et al. 2006; Piro 2007). The thick solid lines show thermal profiles near the end of the simmering.

The simmering phase ends when sub-sonic convection can no longer transport the heat outwards because the timescale of heating is now less than the convective overturn timescale. Since the overturn timescale depends on the integrated energy generation rate near the WD center (while we desire a local measure of when convection should end for simplicity), we assume that this occurs when  $t_h \sim t_{\text{dyn}} \equiv (G\rho_c)^{-1/2}$ , the dynamical timescale. This gives reasonable agreement to other more careful calculations that find the simmering phase ends when  $T_c \approx 8 \times 10^8$  K (Woosley et al. 2004). We plot  $t_h = 10t_{\text{dyn}}$  as a dotted line in Figure 1 to indicate where simmering ends, since the strong temperature sensitivity of  $^{12}\text{C}$  fusion makes this line rather insensitive to the choice of prefactor. If the simmering phase ends earlier, it can be considered in the context of our models by just truncating our results at a slightly lower  $T_c$ .

### 2.1. Main Reaction Cycle at Early Times

At early times, only  $^{12}\text{C}$ ,  $^{16}\text{O}$ , or  $^{22}\text{Ne}$  are potential proton capture nuclei. We compared these rates using Caughlan & Fowler (1988), including strong screening (Salpeter & van Horn 1969). The  $^{16}\text{O}(p, \gamma)^{17}\text{F}$  reaction is negligible, whereas resonances in the  $^{22}\text{Ne}(p, \gamma)^{23}\text{Na}$  reaction make its rate comparable to  $^{12}\text{C}(p, \gamma)^{13}\text{N}$ . However, the larger abundance of  $^{12}\text{C}$  means that it captures more protons by a factor of  $(22/12)X(^{12}\text{C})/X(^{22}\text{Ne}) \approx 40$ . The fate of the synthesized  $^{13}\text{N}$  requires some discussion, as the branching amongst the three relevant reactions:  $^{13}\text{N}(e^-, \nu_e)^{13}\text{C}$ ,  $^{13}\text{N}(\gamma, p)^{12}\text{C}$ ,  $^{13}\text{N}(p, \gamma)^{14}\text{O}$ , depends on  $T$ ,  $\rho$ , and proton mass fraction,  $X_p$ .

The production of protons is always the rate limiting step, so that each proton is almost immediately captured by  $^{12}\text{C}$ . This means that we can find  $X_p$  by balancing the proton production rate from carbon fusion,  $\lambda n_{12}^2 \langle \sigma v \rangle_{12+12}$  (where  $\lambda = 0.44$  is the branching ratio for the reaction  $^{12}\text{C}(^{12}\text{C}, p)^{23}\text{Na}$  and  $n_{12}$  is the  $^{12}\text{C}$  number density) with the proton capture rate,  $n_p n_{12} \langle \sigma v \rangle_{p+12}$ , where  $n_p$  is the proton number density,

$$X_p = \lambda \frac{X(^{12}\text{C}) \langle \sigma v \rangle_{12+12}}{12 \langle \sigma v \rangle_{p+12}}. \quad (2)$$

This is plotted in the upper panel of Figure 2. The small

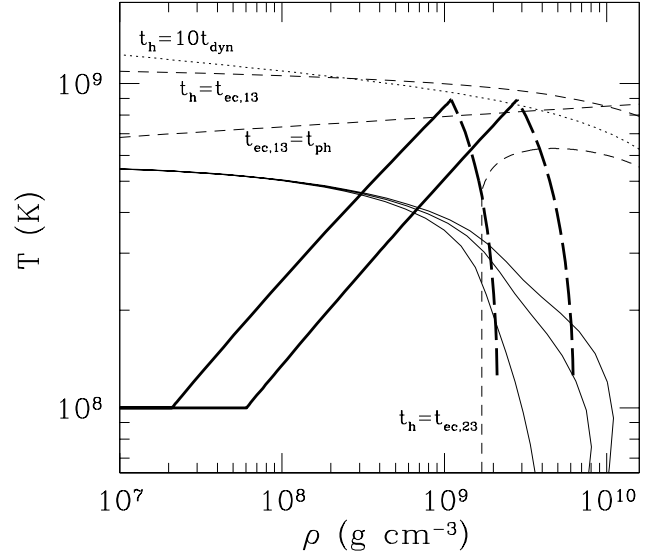


FIG. 1.— Conditions in the simmering WD. Thin solid lines are the range of carbon ignition curves from Yakovlev et al. (2006). The arching thick dashed lines show the central trajectory for the simmering core of a  $1.35M_\odot$  and a  $1.37M_\odot$  WD (left and right, respectively). Thick solid lines are example thermal profiles that are composed of an adiabatic convective core connected to an isothermal exterior. Each case is taken near the end of the simmering phase, which occurs at the dotted line labeled  $t_h = 10t_{\text{dyn}}$ . Dashed lines are crossing points for nuclear reactions described in the text.

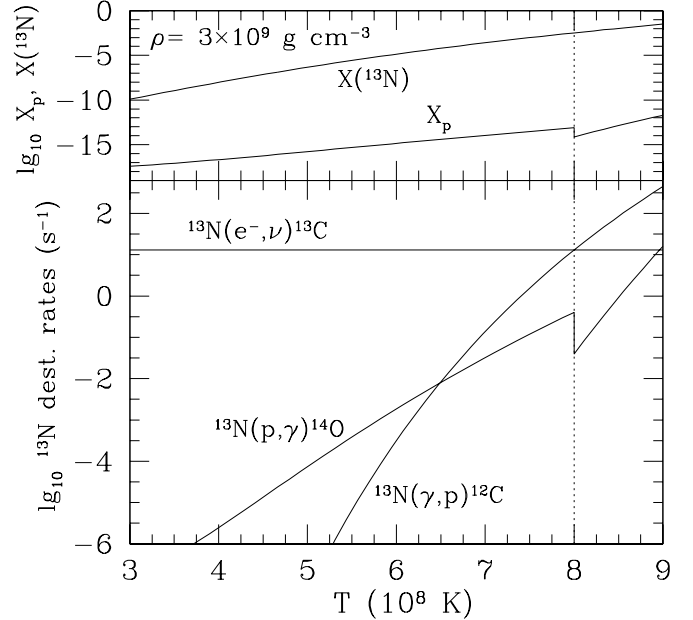


FIG. 2.— Mass fractions  $X_p$  and  $X(^{13}\text{N})$  (upper panel) and  $^{13}\text{N}$  destruction rates (lower panel), versus temperature. The dotted line at  $T = 8 \times 10^8$  K divides where  $^{13}\text{N}$  photodisintegrations becomes important. The density is  $3 \times 10^9 \text{ g cm}^{-3}$  and  $X(^{12}\text{C}) = 0.5$ .

value of  $X_p$  confirms our equilibrium assumption for the proton abundance, and allows us to show that the  $^{13}\text{N}(p, \gamma)^{14}\text{O}$  reaction is negligible (bottom panel of Fig. 2) in comparison to electron captures. The bottom panel also shows the rates for the reactions  $^{13}\text{N}(e^-, \nu_e)^{13}\text{C}$  and  $^{13}\text{N}(\gamma, p)^{12}\text{C}$ , making it clear that electron capture dominates for  $T < 8 \times 10^8$  K.

All of the  $^{13}\text{N}$  comes from the protons synthesized by car-

TABLE 1  
 REACTION SUMMARY FOR MAIN CYCLE

Reaction	Thermal Energy Release (MeV)
$^{12}\text{C}(^{12}\text{C}, p)^{23}\text{Na}$	2.239
$^{12}\text{C}(^{12}\text{C}, \alpha)^{20}\text{Ne}$	4.617
$^{12}\text{C}(p, \gamma)^{13}\text{N}$	1.944
$^{13}\text{N}(e^-, \nu_e)^{13}\text{C}$	0
$^{13}\text{C}(\alpha, n)^{16}\text{O}$	2.214
$^{12}\text{C}(n, \gamma)^{13}\text{C}$	4.947
$^{23}\text{Na}(e^-, \nu_e)^{23}\text{Ne}^a$	0

<sup>a</sup> This reaction only occurs when  $t_h > t_{\text{ec},23}$  (Fig. 1).

bon fusion, therefore the  $^{13}\text{N}$  production rate is equal to that of protons. Once again, this is the slowest step so that we can find the  $^{13}\text{N}$  abundance by balancing  $n_p n_{12} \langle \sigma v \rangle_{p+12} = R_{\text{ec}}(^{13}\text{N}) n_{13}$ , where  $R_{\text{ec}}(^{13}\text{N})$  is the  $^{13}\text{N}$  electron capture rate. Captures into excited states are unlikely to be dominant, allowing us to use the measured  $ft = 4.65 \times 10^3$  s from the ground-state transitions. (Likewise, we use  $ft = 1.91 \times 10^5$  s for  $^{23}\text{Na}$  electron captures in §2.2.) Combining with equation (2) gives

$$X(^{13}\text{N}) = \lambda \frac{13}{12^2} [X(^{12}\text{C})]^2 \frac{\rho N_A \langle \sigma v \rangle_{12+12}}{R_{\text{ec}}(^{13}\text{N})}, \quad (3)$$

where  $N_A$  is Avogadro's number, which is shown in the top panel of Figure 2. The network is completed by  $^{13}\text{C}(\alpha, n)^{16}\text{O}$  and  $^{12}\text{C}(n, \gamma)^{13}\text{C}$ , leading to a composition of one each of  $^{13}\text{C}$ ,  $^{16}\text{O}$ ,  $^{20}\text{Ne}$ ,  $^{23}\text{Na}$ .

There are two complications. The first is at high  $T$ 's where photodisintegration of  $^{13}\text{N}$  happens faster than the electron captures (above the dashed curve labeled by  $t_{\text{ec},13} = t_{\text{ph}}$  in Fig. 1). Chemical balance ( $p + ^{12}\text{C} \leftrightarrow ^{13}\text{N} + \gamma$ ) is achieved in this limit, fixing the proton to  $^{13}\text{N}$  ratio. The  $^{13}\text{N}$  is then slowly removed due to electron captures. The electron captures must always balance the proton production, so the  $^{13}\text{N}$  abundance remains identical to equation (3). Hence, photodisintegration adds steps to the reaction chain (and alters the proton density; top panel of Fig. 2) but does not modify the conclusion that all protons released in  $^{12}\text{C}$  burning lead to  $^{13}\text{N}$  electron capture.

The second complication is the reaction  $^{23}\text{Na}(e^-, \nu_e)^{23}\text{Ne}$  at high densities ( $\rho > 1.7 \times 10^9$  g cm<sup>-3</sup>). This occurs to the right of the dashed line labeled as  $t_h = t_{\text{ec},23}$  in Figure 1, illustrating that these electron captures only take place at certain times during the simmering phase, which we account for in §3. Electron captures on  $^{13}\text{N}$  would not have time to occur above the dashed line labeled  $t_h = t_{\text{ec},13}$  in Figure 1, but this is always after the explosion.

The main reaction cycle is summarized in Table 1. Six  $^{12}\text{C}$  are consumed, producing  $^{13}\text{C}$ ,  $^{16}\text{O}$ ,  $^{20}\text{Ne}$ , and depending on  $t_h$ , either  $^{23}\text{Ne}$  or  $^{23}\text{Na}$ . Therefore, during each cycle either one or two protons have been converted to neutrons.

## 2.2. Late Time Truncation of Neutron Production

The carbon burning ashes eventually become abundant enough to compete with  $^{12}\text{C}$  for proton captures. The relevant products are  $^{20}\text{Ne}$ , and either  $^{23}\text{Na}$  or  $^{23}\text{Ne}$ . The  $^{20}\text{Ne}$  reactions of  $^{20}\text{Ne}(p, \gamma)^{21}\text{Na}$  and  $^{20}\text{Ne}(p, \alpha)^{17}\text{F}$  are negligible, so we focus on  $^{23}\text{Na}$  and  $^{23}\text{Ne}$ .

We plot the proton destruction rate for the most relevant reactions in Figure 3 as a function of  $f$ , the fraction of  $^{12}\text{C}$

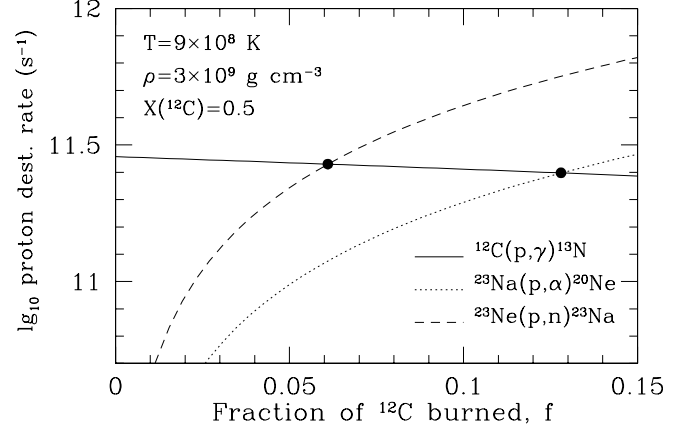


FIG. 3.— The proton destruction rates for different processes as a function of the fraction of  $^{12}\text{C}$  that has burned,  $f$ . The number density of  $^{23}\text{Na}$  or  $^{23}\text{Ne}$  is taken to be  $f n_{12}/3$ . Circles denote crucial places where the proton destruction mechanism switches.

that has burned. The number density of either  $^{23}\text{Na}$  or  $^{23}\text{Ne}$  is taken to be equal to the number density of  $^{12}\text{C}$  burned times  $2/3 \times \lambda \approx 1/3$ . Circles denote where the rates cross each other, which is nearly independent of  $\rho$ . For  $t_h < t_{\text{ec},23}$ ,  $f$  must exceed  $\approx 0.13$  before the  $^{23}\text{Na}(p, \alpha)^{20}\text{Ne}$  reaction becomes important, and ends neutronization.

When  $t_h > t_{\text{ec},23}$ ,  $^{23}\text{Ne}$  forms, which has a higher proton capture cross section than  $^{23}\text{Na}$ . Burning only  $f = 0.061$  is enough that  $^{23}\text{Ne}(p, n)^{23}\text{Na}$  becomes the primary proton sink. Since this makes  $^{23}\text{Na}$  and liberates a neutron, the new  $^{23}\text{Na}$  may electron capture again to make  $^{23}\text{Ne}$ , and the reaction chain  $^{23}\text{Ne}(p, n)^{23}\text{Na}(e^-, \nu_e)^{23}\text{Ne}$  can repeatedly occur, making many free neutrons. Competing with this process are other reaction chains that burn these neutrons (for example, see Table 6 of Arnett & Thielemann 1985). In this regime, it is difficult for us to estimate all the key nuclear reactions that will take place. Although further neutronization is possible, we cannot follow this without a full reaction network (Chamulak et al. 2007b). Such calculations must also be coupled to a realistic model for the core temperature evolution (such as what we present here).

## 3. MAXIMUM NEUTRONIZATION ESTIMATES

We set  $\eta$  as the number of protons that are converted to neutrons for every six  $^{12}\text{C}$  consumed, so that  $\eta = 2$  ( $\eta = 1$ ) for  $t_h > t_{\text{ec},23}$  ( $t_h < t_{\text{ec},23}$ ), where we approximate  $\lambda \approx 0.5$ . The  $\eta = 2$  case is an upper limit since in parts of the convection zone where  $\rho < 1.7 \times 10^9$  g cm<sup>-3</sup> the  $^{23}\text{Na}$  does not electron capture (and  $^{23}\text{Ne}$  that is mixed to lower densities by convection may decay). The total neutronization is measured via

$$Y_e = \frac{1}{2} - \frac{2X(^{56}\text{Fe})}{56} - \frac{X(^{22}\text{Ne})}{22} - f \frac{\eta X(^{12}\text{C})}{6 \times 12}, \quad (4)$$

which includes the initial  $^{56}\text{Fe}$  and  $^{22}\text{Ne}$  content. Neutronization halts either when the WD explodes or when freshly made heavy elements compete for protons (Fig. 3).

In the case of competition from fresh heavy elements, truncation at high densities occurs when  $f = 0.061$  with  $\eta = 2$ . The maximum change in  $Y_e$  is therefore

$$\Delta Y_{e,\text{max}} = -8.5 \times 10^{-4} \frac{X(^{12}\text{C})}{0.5}. \quad (5)$$

A similar limit pertains at lower densities. One way to exceed this limit in the high density case is if additional reaction chains occur (see §2.2). We show  $\Delta Y_{e,\max}$  as a dot-dashed line in Figure 4, in comparison to the  $\Delta Y_e$ 's that result from  $X(^{22}\text{Ne}) = 0.007$  and  $0.02$  (dotted lines). By coincidence, the maximum effect of neutronization during simmering is comparable to that associated with a solar metallicity.

The other possible limiter of neutronization is the onset of the explosion. The reactions in Table 1 show that  $Q \approx 16$  MeV is released as thermal energy when six carbon nuclei are burned.<sup>2</sup> If we let  $E_c$  be the total thermal content that is within the convective core with respect to the initial isothermal WD, this implies a change  $\Delta Y_e = -\eta E_c m_p / Q M_c$  in a convective core of mass  $M_c$ ,

$$\Delta Y_e = -6.5 \times 10^{-4} \frac{\eta}{2} \frac{E_c}{10^{49} \text{ ergs}} \frac{M_\odot}{M_c}, \quad (6)$$

For this to compete with the  $^{22}\text{Ne}$  contribution, a total energy

$$E_c = 1.4 \times 10^{49} \text{ ergs} \frac{2 X(^{22}\text{Ne})}{\eta} \frac{M_c}{0.02 M_\odot}, \quad (7)$$

or  $7 \times 10^{15}$  ergs  $\text{g}^{-1}$ , must be released prior to the explosion.

Simmering ends when dynamical burning is triggered, requiring  $T_c \approx 8 \times 10^8$  K (Woosley et al. 2004). If the burning occurred within a single zone with the specific heat of §2, then reaching this  $T_c$  would require  $\approx 1.3 \times 10^{16}$  ergs  $\text{g}^{-1}$ , in excess of that implied by equation (7). Of course, in reality the convective zone extends outward, so that little mass is at  $T_c$ . To accurately determine the resulting neutronization, we construct hydrostatic WD models consisting of fully convective cores as described at the beginning of §2. We consider isothermal temperatures of either  $10^8$  K or  $2 \times 10^8$  K. At any given moment there is a well defined  $M_c$  (Lesaffre et al. 2006; Piro 2007), and we evaluate the current thermal content by integrating the specific heat relative to the initially isothermal WD,

$$E_c = \int_0^{M_c} c_p [T(M) - T_i] dM, \quad (8)$$

where  $T_i$  is the isothermal WD temperature. In this way we use our time independent models to find the fraction of carbon that must have burned,  $f$ , and the associated  $\Delta Y_e$  as  $T_c$  and  $M_c$  increase with time. We assume no neutrino losses and thus all  $\approx 16$  MeV of thermal energy contributes to heating.

In Figure 4 we summarize the results of these calculations. In each case, the slope of  $\Delta Y_e$  shows a break at the transition from  $\eta = 2$  ( $t_h > t_{\text{cc},23}$ ) to  $\eta = 1$ . This break occurs later for more massive WDs (Fig. 1), thus these have more neutronization during simmering. Increasing the isothermal temperature decreases  $M_c$ , so that it takes less burning to reach a given  $T_c$ . These fully integrated models make it clear that substantial neutronization occurs prior to the explosion. In comparison to the  $\Delta Y_e$  from  $^{22}\text{Ne}$ , simmering effects dominate if  $X(^{22}\text{Ne}) < 0.013$  or  $Z/Z_\odot \lesssim 2/3$ . This thwarts the occurrence of high  $Y_e$  SNe Ia in low metallicity progenitors.

#### 4. CONCLUSION AND DISCUSSION

<sup>2</sup> Not all of this energy will always go into heating up the core. For example, if the convective Urca process is operating, then it will take more energy (and more carbon burning) to get to sufficient temperatures.

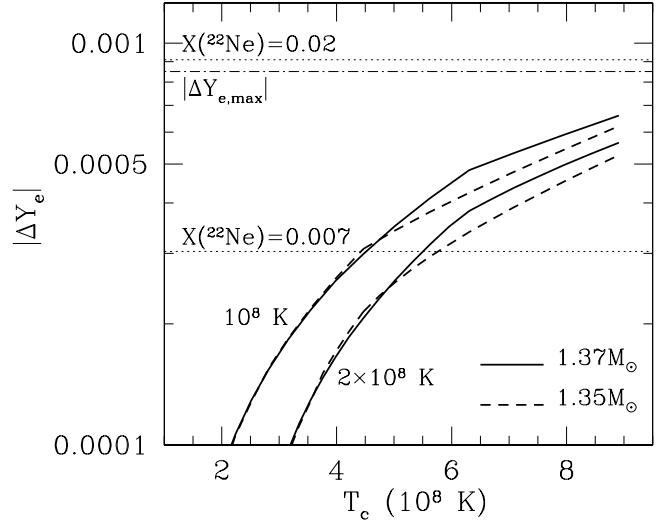


FIG. 4.— Thick dashed ( $M = 1.35M_\odot$ ) and solid ( $M = 1.37M_\odot$ ) lines show the change of  $Y_e$  as a function of the current central temperature,  $T_c$ , due to carbon burning during simmering. In each case we consider isothermal temperatures of  $10^8$  K and  $2 \times 10^8$  K (as labeled). The dot-dashed line is the maximum change possible if proton captures on carbon are only limited by competition from freshly made heavy elements (eq. [5]). Dotted lines bracket the change in  $Y_e$  expected for  $X(^{22}\text{Ne}) = 0.007 - 0.02$ .

We have found that significant neutronization of the WD core occurs throughout the simmering stage of carbon burning until the onset of the explosion. If substantial energy is lost to the convective Urca process (Lesaffre et al. 2005, and references therein), then the neutronization is truncated by proton captures onto freshly synthesized heavy elements (resulting in eq. [5]). The main consequence is a uniform “floor” to the amount of neutronization that dominates over the metallicity dependent contribution for all progenitors with  $Z/Z_\odot \lesssim 2/3$ .

Given the likely significance this has for SNe Ia, more work needs to be done. In particular, at high ignition densities, heavy element electron captures and a full reaction network are needed to follow the resulting diverse collection of elements (see the discussion in §2.2). The convective Urca process is another complication we have not addressed. In principle, if more energy is lost to neutrinos then more burning (and thus more neutronization) is required to make the burning dynamical. Assessing this will necessitate coupling a full nuclear network (Chamulak et al. 2007b) to convective calculations. Such models would accurately determine  $\eta$  rather than simply setting it to 1 or 2.

In closing, we highlight some important features exhibited by recent observations of SNe Ia. It is clear that the amount of  $^{56}\text{Ni}$  produced in SNe Ia has a dynamic range ( $0.1 - 1M_\odot$ ) larger than can be explained by metallicity or simmering neutronization. However, since an intriguing trend is the prevalence of  $^{56}\text{Ni}$  rich events in star-forming regions it is interesting to quantitatively explore how large the observed discrepancy is. Using the SNLS sample of Sullivan et al. (2006), Howell et al. (2007) found that the average stretch is  $s = 0.95$  in passive galaxies (e.g. E/S0’s) and  $s = 1.05$  in star-forming galaxies. Using Jha et al.’s (2006)  $\Delta M_{15}(B) - s$  relation and Mazzali et al.’s (2007) relation between  $\Delta M_{15}(B)$  and  $^{56}\text{Ni}$  mass we get  $0.58M_\odot$  ( $s = 0.95$ ) and  $0.72M_\odot$  ( $s = 1.05$ ). Hence, amongst the large diversity, there is a tendency for SNe in star-forming galaxies to produce  $\approx 0.13M_\odot$  more  $^{56}\text{Ni}$  than those in large ellipticals.

Since the SN Ia rate scales with mass in ellipticals and star formation rate in spirals (Mannucci et al. 2005; Scannapieco & Bildsten 2005; Sullivan et al. 2006), SNe from passive galaxies in the SNLS survey are from more massive galaxies than the SNe in star-forming galaxies (Sullivan et al. 2006). Using the mass-metallicity relation of Tremonti et al. (2004), our integration of the separate samples in Sullivan et al. (2006) yield average  $12 + \log(\text{O}/\text{H}) = 8.87$  in active galaxies and 9.1 in ellipticals (solar value is  $12 + \log(\text{O}/\text{H}) = 8.69$ ). Due to the increase of N/O at high metallicities (Liang et al. 2006), the SNe in ellipticals have twice as much  $^{22}\text{Ne}$  content as those in spirals. From the relation of Timmes et al. (2003), this implies  $\approx 5\%$  less  $^{56}\text{Ni}$ , whereas the observed decrement is  $> 15\%$ . Explaining the observed decrement would require a contrast of  $\Delta X(^{22}\text{Ne}) \approx 0.06$ , or nearly 3 times solar. Although we have found that simmering enhances neutronization, the effect is not great enough ( $\Delta Y_{e,\text{max}}$

would give the same change in neutronization as doubling a solar metallicity), and a diverse set of core conditions would still be required. A large enhancement could be present in the core if substantial gravitational separation had occurred (Bildsten & Hall 2001; Deloye & Bildsten 2002), yet convective mixing during simmering will reduce it based on the fraction of the star that is convective. For a convection zone that extends out to  $M_{\odot}$ , the resulting  $^{22}\text{Ne}$  enhancement would be at most  $\approx 30\%$ .

We thank E. Brown, R. Ellis, F. Forster, A. Howell, B. Paxton, P. Podsiadlowski, H. Schatz and F. Timmes for discussions, and D. Yakovlev for sharing carbon ignition curves. We also thank the referee for constructive comments and questions. This work was supported by the National Science Foundation under grants PHY 05–51164 and AST 02–05956.

## REFERENCES

- Arnett, W. D. & Thielemann, F.-K. 1985, *ApJ*, 295, 589  
 Bildsten, L. & Hall, D. M. 2001, *ApJ*, 549, L219  
 Caughlan, G. R., & Fowler, W. A. 1988, *At. Data Nucl. Data Tables*, 40, 283  
 Chabrier, G. & Potekhin, A. Y. 1998, *Phys. Rev.*, E58, 4941  
 Chamulak, D. A., Brown, E. F., & Timmes, F. X. 2007a, *ApJ*, 655, L93  
 Chamulak, D. A., Brown, E. F., Timmes, F. X., & Dupczak, K. 2007b, submitted to *ApJ*  
 Deloye, C. J. & Bildsten, L. 2002, *ApJ*, 580, 1077  
 García-Senz, D. & Woosley, S. E. 1995, *ApJ*, 454, 895  
 Howell, D. A., Sullivan, M., Conley, A. & Carlberg, R. 2007, *ApJ*, 667, L37  
 Jha, S., et al. 2006, *AJ*, 131, 527  
 Kuhlen, M., Woosley, S. E., & Glatzmaier, G. A. 2006, *ApJ*, 640, 407  
 Lesaffre, P., Podsiadlowski, Ph., & Tout, C. A. 2005, *MNRAS*, 356, 131  
 Lesaffre, P., Han, Z., Tout, C. A., Podsiadlowski, Ph., & Martin, R. G. 2006, *MNRAS*, 368, 187  
 Liang, Y. C., et al. 2006, *ApJ*, 652, 257  
 Mannucci, F., et al. 2005, *A&A*, 433, 807  
 Mazzali, P. A., Roepke, F. K., Benetti, S. & Hillebrandt, W. 2007, *Science*, 315, 825  
 Nomoto, K., Thielemann, F.-K., & Yokoi, K. 1984, *ApJ*, 286, 644  
 Phillips, M. M., Lira, P., Suntzeff, N. B., Schommer, R. A., Hamuy, M., & Maza, J. 1999, *AJ*, 118, 1766  
 Piro, A. L. 2007, submitted to *ApJ*  
 Piro, A. L. & Chang, P. 2007, submitted to *ApJ*  
 Salpeter, E. E., & van Horn, H. M. 1969, *ApJ*, 155, 183  
 Scannapieco, E. & Bildsten, L. 2005, *ApJ*, 629, L85  
 Sullivan, M. et al. 2006, *ApJ*, 648, 868  
 Thielemann, F.-K., Nomoto, K., & Yokoi, K. 1986, *A&A*, 158, 17  
 Timmes, F. X., Brown, E. F., & Truran, J. W. 2003, *ApJ*, 590, L83  
 Timmes, F. X., & Woosley, S. E. 1992, *ApJ*, 396, 649  
 Tremonti, C. A. et al. 2004, *ApJ*, 613, 898  
 Weinberg, N., Bildsten, L., & Schatz, H. 2006, *ApJ*, 639, 1018  
 Woosley, S. E., Kasen, D., Blinnikov, S., & Sorokina, E. 2007, *ApJ*, 662, 487  
 Woosley, S. E., & Weaver, T. A. 1986, *ARA&A*, 24, 205  
 Woosley, S. E., Wunsch, S., & Kuhlen, M. 2004, *ApJ*, 607, 921  
 Wunsch, S. & Woosley, S. E. 2004, *ApJ*, 616, 1102  
 Yakovlev, D. G., Gasques, L. R., Afanasjev, A. V., Beard, M., & Wiescher, M. 2006, *Phys. Rev. C*, 74, 035803